Circular-Polarized Metal-Only Reflectarray With Multi-Slot Elements

Kendrick Q. Henderson, *Student Member, IEEE*, and Nima Ghalichechian, *Senior Member, IEEE*

***Abstract*— A circular-polarized metal-only reflectarray operating at 20 GHz is reported in this article. The reflectarray uses a novel multi-slot element that supports both left-hand and right-hand circular polarization for applications such as satellite communication. The element maintains a full phase coverage of 360° for both polarizations over a wide bandwidth spanning from 18 to 24 GHz (30%). Moreover, the square slot of the element allows the antenna to maintain a low axial ratio (<2 dB) over a large bandwidth. As a result, the 3-dB axial ratio bandwidth far exceeds the 1 and 3 dB gain bandwidths. The maximum simulated loss introduced by the reflectarray element was 0.9 dB at 24 GHz. The measured gain of the fabricated $20\lambda_0$ diameter (300 mm) reflectarray was 31.4 dB with a 1 and 3 dB gain-bandwidth of 6.8% and 10.1%, respectively, for each polarization. Measurement results illustrate excellent agreement with simulation. This reflectarray, which supports both polarizations, has both a polarization diversity and an increased bandwidth for satellite applications.**

***Index Terms*— Circular polarized, dual-polarization, metal-only, reflectarray, slot.**

I. Introduction

REFLECTARRAYS combine the favorable features of both parabolic reflectors and phased array antennas, with the desirable features of high efficiency, high gain, low profile, low weight, and simplicity of the design incorporated within. These electrical and mechanical characteristics make them an excellent candidate for satellite communication and direct broadcasting services (DBSs) [1], [2]. Traditional microstrip technology is used to create reflectarrays, with the patch antenna array printed onto a low loss dielectric substrate. As the aperture of a reflectarray can be quite large, both in terms of wavelength and physically, the substrate can make the design prohibitively expensive. In addition, the introduction of dielectric material into a harsh space environment can lead to a decrease in antenna performance [3]. To prevent radiation and thermal stresses on the antenna, a radome can be used at the expense of the increase in weight, height, and cost.

Manuscript received July 7, 2019; revised April 15, 2020; accepted April 17, 2020. Date of publication May 14, 2020; date of current version September 3, 2020. This work was supported in part by the Department of Defense SMART Program, in part by the Naval Surface Warfare Center (NSWC) Crane Division, and in part by the ElectroScience Laboratory Consortium on Electromagnetics and the Radio Frequencies (CERF). *(Corresponding author: Kendrick Q. Henderson.)*

The authors are with the ElectroScience Laboratory, The Ohio State University, Columbus, OH 43212 USA (e-mail: henderson.965@osu.edu; ghalichechian.1@osu.edu).

Color versions of one or more of the figures in this article are available online at http://ieeexplore.ieee.org.

Digital Object Identifier 10.1109/TAP.2020.2993229

To circumvent these problems, a metal-only reflectarray is a superior alternative for satellite communication and DBS. Metal-only reflectarrays completely remove the dielectric substrate from the antenna, the elements of which are machined into a high strength and corrosive-resistant metal sheet such as stainless steel or aluminum [4], [5]. The use of a metal-block element with an adjustable height is another also effective method, through which the reflectarray element achieves a full 360° of phase coverage [6]. Unfortunately, the design is heavier with a thicker profile as compared to planar arrays. Another example used a concept similar to a tunable height metal-block [7]. Rather than changing the block height, a rectangular groove is cut into the block at a variable height. Although the method did yield full phase coverage with reduced weight, the large design profile of the design was still a major drawback.

Currently, very little research has been undertaken in terms of fabricating metal-only reflectarrays, with most of the literature focusing on slot-based elements with very limited phase coverage, typically less than 300° [4]. Although the reflectarray elements of [5], [8], [9] overcame this limitation by an increase in the phase coverage to a full 360,° it was effective only for linear polarizations. Therefore, the failure of these designs to support circular polarization greatly limits their use in both satellite communication and DBS.

Circular polarization is used for both polarization diversity and to reduce the effect of the earth's atmosphere on the communication link. In a linear-polarized system, the antenna must maintain alignment between the receiver and transmitter to maintain an acceptable signal level. This is less of a problem for a circularly polarized antenna as the power received by the antenna does not depend on the orientation. Although the reflectarray element in [10] was a circular polarized metal-only element, it exhibited an unstable phase response over the proposed bandwidth of 14.5–16.75 GHz (14.4%) that ranged from 320° to 402°. The limited number of metal-only reflect arrays available that are circular polarized has thus required the incorporation of a dielectric substrate to support the traditional patch elements for circular polarization. Unfortunately, increases in costs, complexity, sources of failure, and antenna loss have been the result.

In this article, the authors propose a multi-slot element that has both 360° of phase coverage, over the entire bandwidth of 18–24 GHz (30%), and is circularly polarized. The element supports both left-hand circular polarization (LHCP) and right-hand circular polarization (RHCP) as previously reported in our preliminary design [11]. This new type of

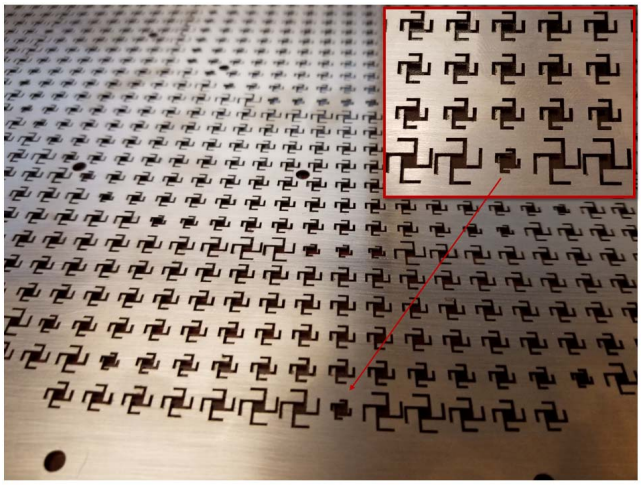

Fig. 1. Overview of the top layer of the circularly polarized reflectarray with multi-slot elements.

multi-slot element design, which allows the antenna to support either LHCP, RHCP, or both, to potentially double the usable bandwidth for the communication system. Fig. 1 shows the top surface of the proposed array with the aforementioned slot elements.

Section II details the design and analysis of the unit element. Section III details the simulation of a $20\lambda_o$ diameter finite reflectarray using an array theory in which the phase map is calculated at the operating frequency of 20 GHz. A full-wave model of a reflectarray with the novel multi-slot element was constructed to determine the reflectarray properties such as gain and axial ratio. The results of that effort are reported in Section IV. The simulated reflectarray was subsequently fabricated to verify this design, with the measurement results discussed in Section VI. A comparison between the results of the simulated design, fabricated design, and other work on the topic is presented in Section VII. Finally, in Section VIII, a conclusion is provided.

II. Unit Cell Design and Analysis

The design of the metal-only reflectarray element must support both LHCP and RHCP while maintaining full phase coverage of 360° over the desired bandwidth. This means the axial ratio of the antenna must be low—typically well below 3 dB—for the desired bandwidth as well. Although the analysis conducted by Wenxing *et al.* [4] shows that square slot can support both LHCP and RHCP, the element has no phase coverage. This absence of phase coverage is due to the inherent wideband structure of this square slot rather than a sharp resonance near its design frequency. Therefore, the slot never reaches a point of resonance without extending pass the bounds of the unit cell [1]. To preserve the polarization of the square slot and extend the phase range, this article introduces additional slots—with variable length—at the four corners of the center square slot. Hence, this formation introduces a resonance near the desired operating frequency. As shown later in this section, the element operates over the wide bandwidth of 18–24 GHz (30%) and supports both LHCP and RHCP.

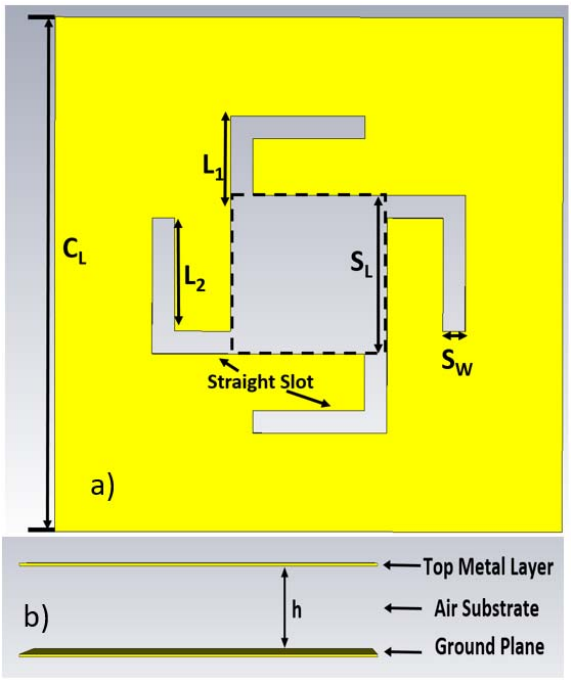

Fig. 2. (a) Top view of the element showing the center square slot and the adjustable straight slots on its corners. (b) Side view of the element showing the top surface and the ground layer (yellow represents metal).

TABLE I
Geometry of the Proposed Metal-Only Element

Description	Parameter Name	Values (mm)
Space between elements	C_L	7.50
Straight slot length	L_1, L_2	0.3-1.98
Square slot length	S_L	2.31
Straight slot width	S_W	0.45
Air gap	h	4

Despite the added electromagnetic functionality provided by the addition of the four corner slots, the fabrication of the array remains relatively simple.

The proposed multi-slot element is shown in Fig. 2. As illustrated in Fig. 2(a), the element consists of a square slot at the center of the unit cell and four L-slots, each of which is composed of two connected straight slots of different physical lengths with each L-slot of equal electrical length. The length of the L-slots is adjusted to tune the phase of the element, the geometry of which is shown in Table I. These parameters, which are for a designed frequency of 20 GHz, are configurable to other frequencies if needed. While the center-slot element size is kept constant, both L_1 and L_2 of the corner slots are exploited for changing the phase of the elements. The selected spacing between the elements C_L was 7.5 mm or $0.5\lambda_o$, with λ_o representing the free-space wavelength at 20 GHz. The selected width of the straight slots, S_W, was 0.45 mm for ease of fabrication. The metal of choice was stainless steel, a commonly used sheet metal, with a thickness of 0.529 mm (0.020 in). It is a commodity of choice in terms of availability, cost, mechanical and chemical

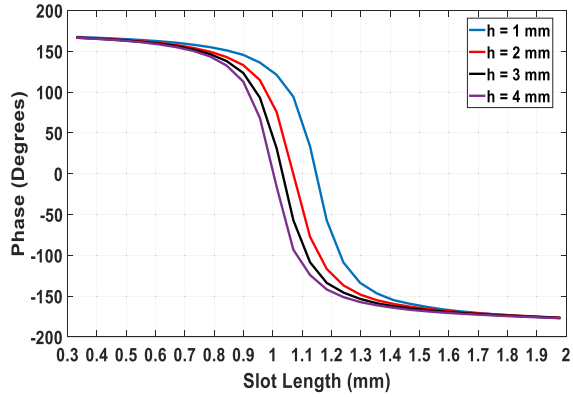

Fig. 3. Reflected phase of the spiral slot element as a function of slot lengths L_1 and L_2. The separation h of the element was changed to analyze the element's susceptibility to manufacturing tolerance.

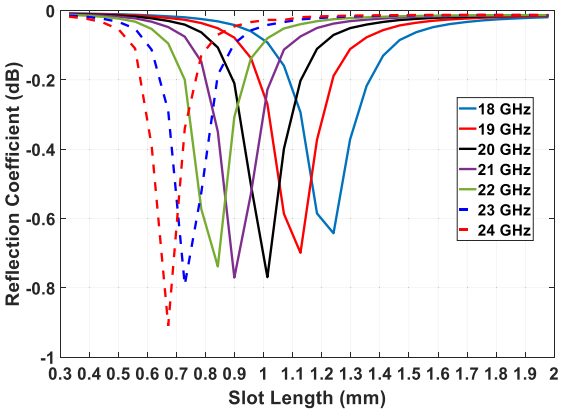

Fig. 5. Reflection coefficient of the spiral slot element as a function of slot lengths L_1 and L_2. The phase of the element was again scanned over frequency.

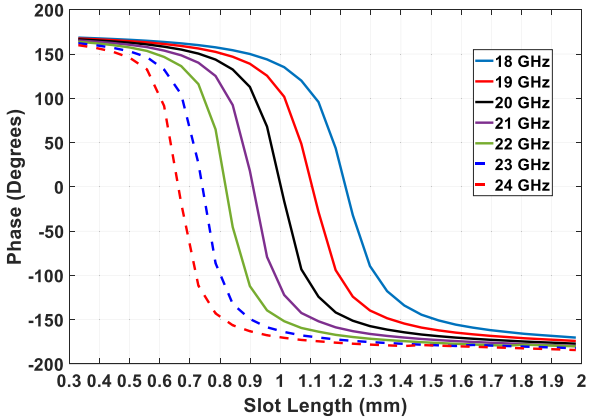

Fig. 4. Reflected phase of the spiral slot element as a function of slot lengths L_1 and L_2. The phase of the element was scanned over frequency.

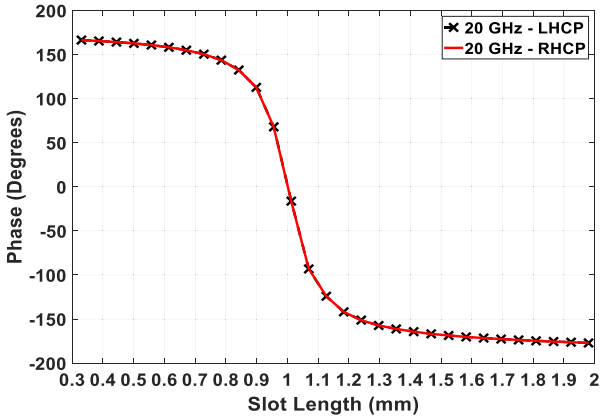

Fig. 6. Reflected phase of the spiral slot element as a function of slot lengths L_1 and L_2. The element was excited with both LHCP and RHCP waves. The phase response of both match so the element supports both.

properties, mechanical strength for structural support, and resistance to chemical corrosion. The conductivity used during the simulation of the infinite array was 7.69×10^6 S/m with an infinite array used to account for the mutual coupling between adjacent elements. CST Microwave Studio was used to simulate the unit cell and resulting finite array of this article. Later in Section IV, we will discuss the full-wave simulation of the entire array composed of 1256 elements.

To determine the air gap distance between the two metals, an analysis was performed to determine the sensitivity of the phase response of the element to the air gap distance. In Fig. 3, L_1 and L_2 were varied as the height of the reflectarray element was changed. As the air gap distance increased, the steepness of the phase curve decreased, at which point the phase curve approached asymptote. The results thus informed the selection of a 4 mm air gap distance to the reduce phase error during fabrication and to keep the profile of the antenna small.

Once h was determined, the phase response and magnitude of the reflection coefficient was simulated over 18–24 GHz. In Fig. 4, the phase response is a full 360° over the wide bandwidth with parallel phase curves. Fig. 5 shows the reflection coefficient (S_{11}) for the stainless-steel reflectarray element. The minimum value of -0.9 dB occurred at 24 GHz. Although small, it is possible to reduce this loss with a higher conductivity material such as copper or aluminum over stainless steel.

An important metric for our design is the ability to support both LHCP and RHCP. In another simulation (as detailed in Fig. 6), the element was excited with both LHCP and RHCP waves. Note that the reflected phase curves of the polarizations align completely with each other, indicating that our unique element shape supports both polarizations with no difference in their respective reflected phase.

To gain greater insight as to how the element supports both polarizations, the electric field within the slots are simulated and analyzed. In Fig. 7, the electric field is shown over the full phase cycle. The arrows of the plot indicate the direction of the electric field as the phase progress from 0° to 270°. The L-slots are excited by the vertical and horizontal components of the incident electric field. As the phase progresses, the maximum point of excitation switches between the vertical and horizontal slots. Note that the square slot allows the electric field to switch between the set of L-slots while maintaining a low axial ratio. The field lines along the edge of the square slot show that the reflected field moves along the edge to the other pair

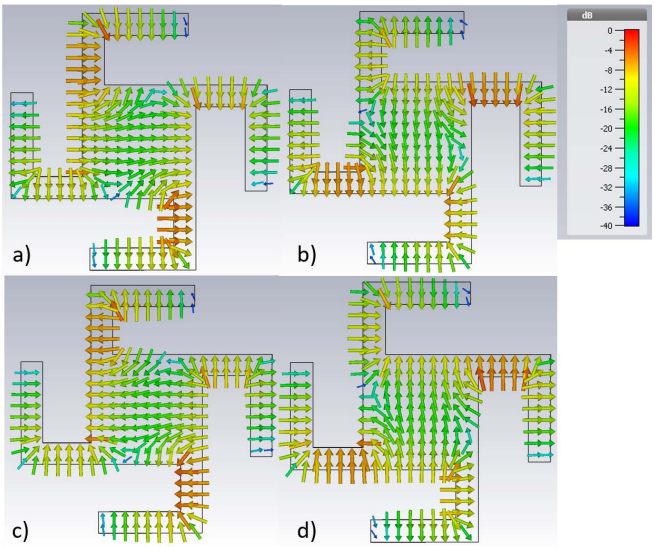

Fig. 7. Simulated electric field inside the spiral slot as it progresses over phase. The electric field phase changes from (a) 0°, (b) 90°, (c) 180°, to (d) 270°.

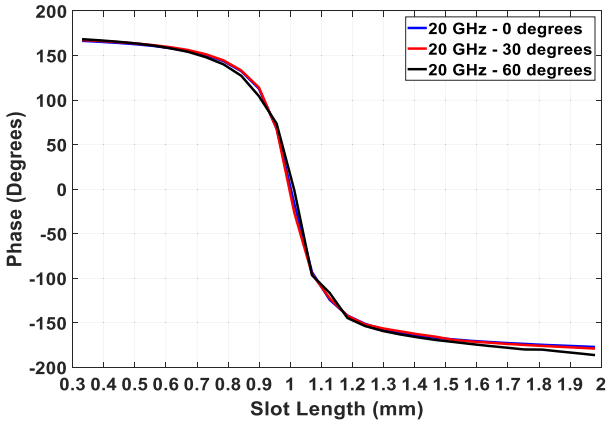

Fig. 8. Reflected phase of the spiral slot element as a function of slot lengths L_1 and L_2. The phase response of the element shows very little change with an increase in incident angle.

of L-slots for the other axis. A low axial ratio is possible as the transition between each axis is gradual rather than sharp, which is very different from the sharp transition caused by either the cross or the multi-slot element previously [10]. Since a circularly polarized field is the summation of two linear polarized fields, the field distribution on the element's surface will be the same for the other circular as it is in Fig. 7. The proposed unit cell takes advantage of the nature of circularly polarized fields.

The observed stable phase curve over wide incident angel in the reflectarray element is an important metric as the size of the reflectarray determines the largest incident angle for the edge elements. As indicated by the maximum angle of 60° in the phase curve in Fig. 8, the element shows very little variation as a function of the incident angle.

III. Reflectarray Design

Upon analysis of the parameters and metrics of the unit cell, a fixed-beam reflectarray was designed to evaluate the performance of the unit cell within a finite array. It was then possible to use this simulation to determine the resulting gain, bandwidth, axial ratio, and efficiency using the reflection coefficient of the unit cell.

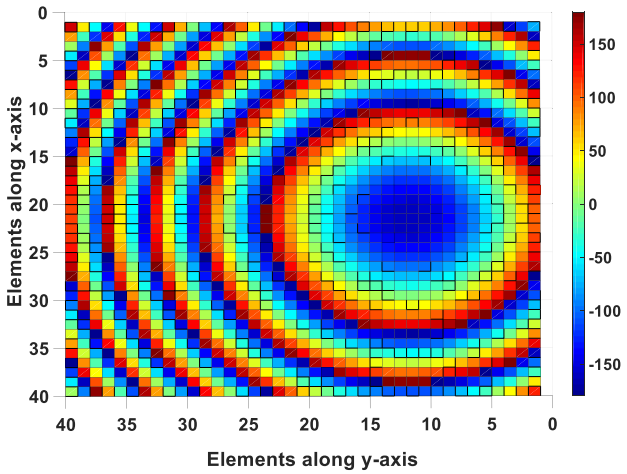

Fig. 9. Required reflected phase of the unit cells to create a beam that is normal to the reflectarray with the requirements in Table II.

The reflectarray was designed with an offset conical feed horn of 15° to avoid feed blockage. This feed horn, used to excite the circularly polarized waveforms, was modeled via a $\cos^q\theta$ function with the q value of 13.5. This result correlates to the 30° beamwidth of the test feed horn for the reflectarray. The beam pattern for the offset horn was used to calculate the feed-to-diameter ratio of the reflectarray for maximum theoretical efficiency, which was determined by comparing the surface illumination and spillover efficiencies from the horn relative to the aperture size [12], [13]. The selected feed-to-diameter ratio was 0.94, which correlates to an efficiency of 73%. The feed-to-diameter ratio and offset angle resulted in an (x, y, z) phase location of (0, 84.3, and 314.9 mm), respectively.

To build a beam with an angle normal to the reflectarray surface, the phase of each element was determined using the well-known array theory. The feed horn illuminates the surface of the reflectarray with a magnitude and phase gradient. The reflectarray elements must introduce a phase change to create and direct the desired beam [14]–[17]. The following equation shows the phase that each element must introduce to create a narrow-steered beam

$$\varphi_{mn} = k_0(d_{mn} - (x_{mn}\cos\varphi + y_{mn}\sin\varphi)\sin\theta). \quad (1)$$

The parameters used in the equation are the propagation constant of free space (k_0), the distance between the feed horn's phase center (d_{mn}) and the unit cell, the distance between the unit cell and the coordinate origin of the reflectarray (x_{mn}, y_{mn}), and the desired beam direction (φ,θ). The calculated phases of the reflectarray elements are shown in the contour of Fig. 9. These phases are combined with the illumination taper (I_{mn}) and spatial delay of the feed horn in (2) to find calculate the resulting

TABLE II
PARAMETERS OF FINITE REFLECTARRAY

Center Frequency	20 GHz
Horn Type	Conical
Horn Gain	15.9 dB
Horn Beamwidth	30°
Reflectarray Diameter	$20\lambda_o$
Feed-to-Diameter	0.94
Feed offset	15°
Feed Location (x, y, z)	0 mm, 84.3 mm, 314.9 mm
Main Beam Direction (θ, φ)	0°, 0°

radiation

$$E(\theta,\varphi)=\sum_{m=1}^{M}\sum_{n=1}^{N} I_{mn}\times e^{-jk\left(|r_{mn}-r_f|-r_{mn}*\hat{u}\right)}e^{j\varphi_{mn}}. \quad (2)$$

The horn of the reflectarray is on the right side of the plot at the middle of the x-axis. The key design parameters are shown in Table II.

IV. FULL WAVE REFLECTARRAY SIMULATION

The full-wave CST Microwave Studio software was used for the reflectarray simulation with the integral solver for the design simulation. Since the reflectarray contains 1256 individual elements with different geometries, in-house automation software was used to create the $20\lambda_o$ reflectarray geometry in CST. This software uses the parameters from Table I, the 20 GHz phase curve from Fig. 4, and the calculated phase map of Fig. 9. Combining this information allows the software to know the required individual slot length at each unit cell to reflect the incident field with the correct phase shift [18]. The reflectarray was then imported onto a dedicated simulation server, as the electrically large $20\lambda_o$ reflectarray is computationally intensive.

Since this reflectarray is designed to radiate both LHCP and RHCP, the feed of the antenna must be circularly polarized. A conical horn with a square waveguide aperture was used to create the LHCP and RHCP waves that excite the feed horn. A rectangular waveguide was attached and turned 90° to simulate the vertical and horizontal components of the CP wave. The results were combined in post-processing in CST to ensure that the axial ratio of the feed horn did not limit the axial ratio of the reflectarray over the bandwidth of interest. The simulated reflectarray and results of the 3-D pattern for an LHCP beam are shown in Fig. 10. As mentioned in Section III, the feed horn is positioned at a 15° offset from the z-axis.

The radiation pattern in the two principal planes, xz and yz, are plotted in Figs. 11 and 12, respectively. Note that the simulated reflectarray has a narrow main beam, with a peak gain of 32.5 dB for both LHCP and RHCP and low sidelobes. There is also good agreement between the array theory and simulation as the main beam is at the desired location (normal to the surface). In the xz plane, the reflectarray's half-power beamwidth (HPBW) was 3.3° with a sidelobe level (SLL) that was 24 dB lower than the main beam. In the yz plane, the HPBW was 3.4° with an SLL of 24 dB. The gain-frequency results shown in Fig. 13 illustrates that the antenna has its

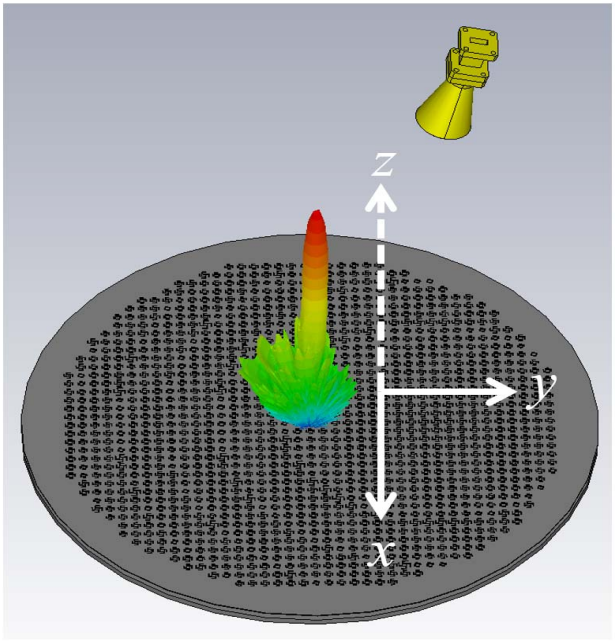

Fig. 10. $20\lambda_o$ metal-only reflectarray using the spiral slot element. The feed horn was placed at a focus-to-diameter ratio of 0.94 with a 15° tilt. The beam is placed at $\theta = 0°$ and $\varphi = 0°$ or normal to the surface.

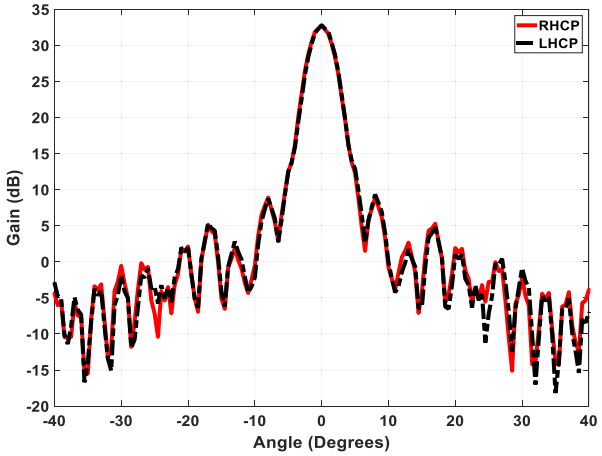

Fig. 11. Radiation patterns for the simulated reflectarray for both RHCP and LHCP at 20 GHz. The radiation patterns are cut along the xz plane. The HPBW was 3.3°.

maximum gain point at the designed frequency of 20 GHz. The gain for both polarizations closely matches each other. This conforms to the array theory as the antenna's unit cell phases were designed for 20 GHz. The 1 and 3 dB gain-bandwidth were 6.5% and 10%, respectively, for both polarizations.

The axial ratios for both polarizations, shown in Fig. 14, is an important metric for a circularly polarized antenna as it determines the true bandwidth for the antenna. If the antenna's axial ratio is above 3 dB for its band of operation, it is no longer circular polarized, as one component of the circularly polarized waveform now has a much higher magnitude than the other. Hence, those antennas effectively become linearly polarized. The simulated axial ratio for our array is below 2 dB for 18–22 GHz and only reaches 3 dB at 23.5 GHz,

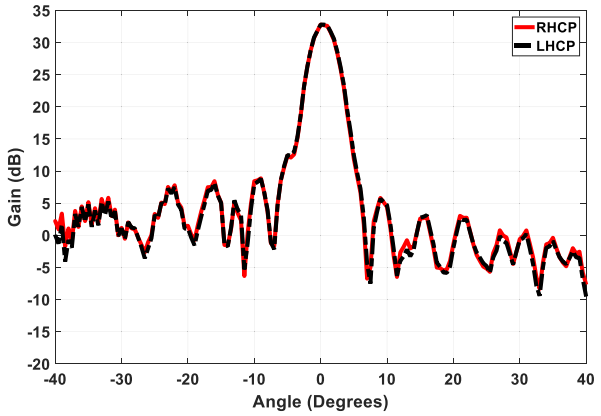

Fig. 12. Radiation patterns for the simulated reflectarray for both RHCP and LHCP at 20 GHz. The radiation patterns are cut along the *yz* plane. The HPBW was 3.4°.

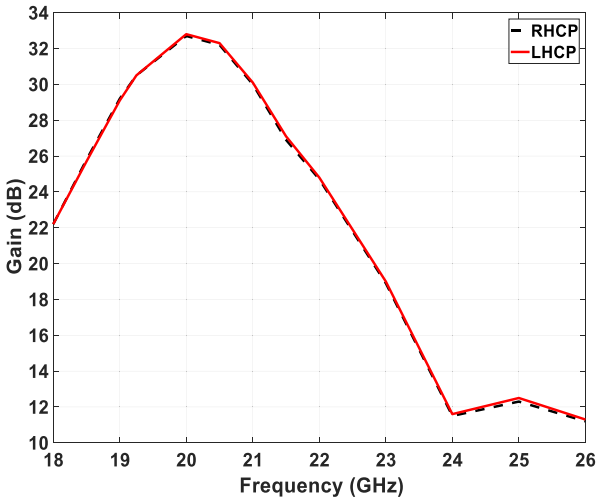

Fig. 13. Gain as a function of frequency for the simulated reflectarray for both RHCP and LHCP.

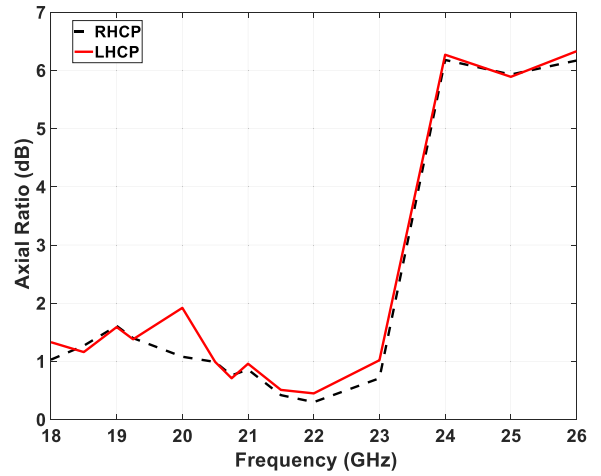

Fig. 14. Axial ratio of the simulated reflectarray for both RHCP and LHCP.

resulting in 5.5 GHz of bandwidth for the axial ratio. The novel design of the reflectarray unit cell, which maintains the axial ratio well below 3 dB for a wide bandwidth, is the reason

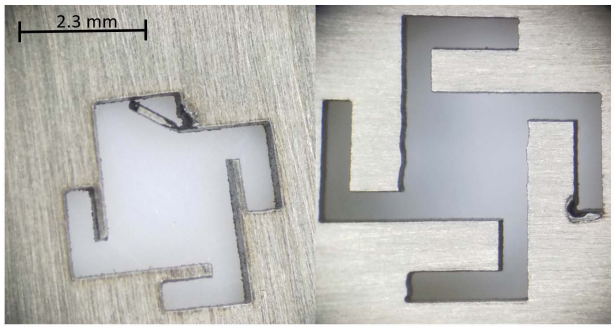

Fig. 15. Fabrication defects of the reflectarray. The smaller elements had noticeable defects due to the initiation point for each laser cut.

Fig. 16. Two pieces of sheet metal of the metal-only reflectarray. The ground plane (left) and the laser-etched top layer (right) have a series of holes drilled in them.

for this superior performance. Therefore, the axial ratio is not a concern for this antenna as it's larger than its 1 or 3 dB frequency bandwidth. To conclude, an antenna that supports both LHCP and RHCP over its bandwidth of operation was successfully simulated.

V. Fabrication and Assembly

To verify the design, the simulated reflectarray was fabricated and assembled. First, 1256 distinct cells were laser-machined into the top stainless-steel layer surface (shown in Fig. 1). This laser etching process had a tolerance of 0.0245 mm or 0.001 of an inch, which is very accurate for our 20 GHz design, which produces an average phase error of 4.3° over the full tuning range of the spiral slot. After fabrication, the top layer was inspected. While the majority of the elements were defect-free, some defective cells were found along the surface as shown in Fig. 15. A greater degree of defects was observed in the smaller slots than the larger slots near the 2 mm limit of the multi-slot's tunable range. The result is a potential for minor phase errors, and consequent minor impacts on the gain pattern for the fully assembled array.

In addition to the top plate, the other components of the reflectarray assembly include the ground plane, rotator plate, dielectric screws/spacers, horn, and horn fixture. Similar to the top metal, the ground in Fig. 16 is made of stainless steel with a thickness of 3.175 mm (one-eighth of an inch). The particular thickness of this commonly available metal was chosen as it adds to the structural integrity of the antenna assembly. The same pattern was drilled into both the ground plane and the top metal layer, with high-strength polyethylene dielectric screws

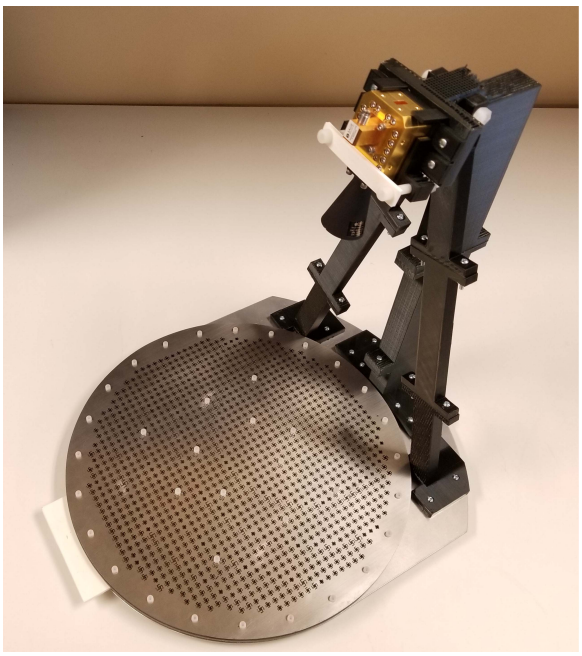

Fig. 17. Assembled reflectarray composed of the top laser-etched layer, ground plane, rotator plate, and 3-D printed feed structure. The reflectarray used an orthomode transducer to test the axial ratio of the unit cell.

used to connect them. To ensure that the gap between the top metal layer and the ground plane was 4 mm across the entire large array, a series of nylon dielectric spacers was added around each screw.

A rotator plate was fabricated to mount the array in the anechoic chamber. This plate was used for mechanical support and testing purposes only and had no adverse effect on the electromagnetic performance of the array. As a result, this plate attaches the antenna to the measurement system in the anechoic chamber to hold the feed assembly in place. The rotator plate was of the same diameter as the reflectarray with an added extension. The outer edge extension on one side provides a robust platform for bolting the feed horn assembly.

The fully assembled reflectarray is shown in Fig. 17. The feed assembly was made of a 3-D-printed polylactic acid (PLA) material for rapid prototyping. The parts support the feed horn from three separate PLA cantilever posts. The horn is a standard gain circular polarized horn with 15 dB of gain (18–26.5 GHz). An orthomode transducer (model # SAT-FK-42042-S1, Sage Millimeter, Inc.) is attached to the feed horn to excite both vertical and horizontal polarizations. This transducer facilitates testing without the need of rotating the feed horn during gain measurements, thus avoiding any spatial or angular errors, and eliminating an important source of measurement error. The orthomode transducer does, however, induce a small insertion loss of 0.5 dB for each linear polarization (the transducer has two linear ports feeding a circular horn). Therefore, the measured linear polarizations from each feedline were added—in post-processing—to extract the total circular polarized gain.

VI. Measurement and Verification

After assembly of the reflectarray, the antenna was mounted on the column in the anechoic chamber where both linear

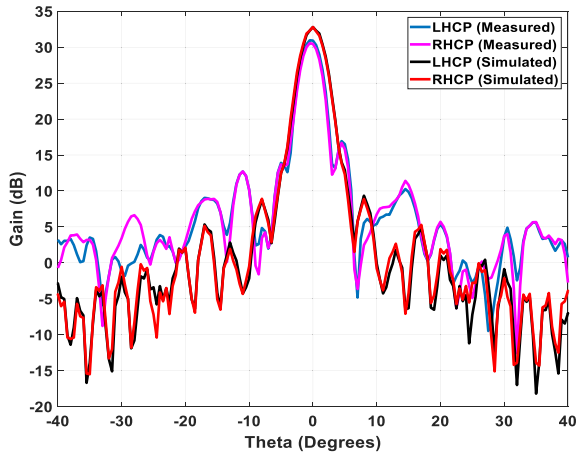

Fig. 18. Absolute value radiation patterns for the measured reflectarray for both RHCP and LHCP at 20 GHz. The radiation patterns are measured along the *xz* plane. The measured HPBW was 3.3°.

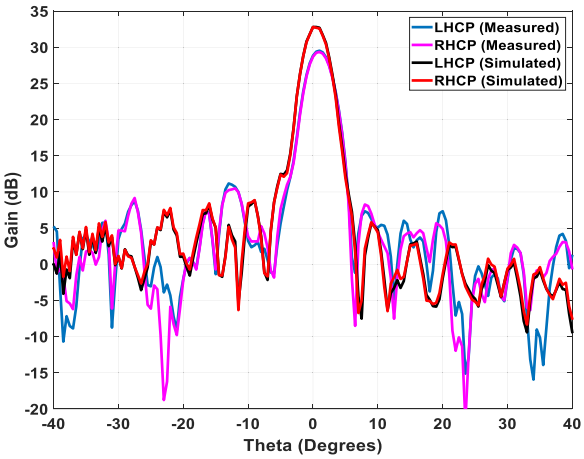

Fig. 19. Absolute value radiation patterns for the measured reflectarray for both RHCP and LHCP at 20 GHz. The radiation patterns are measured along the *yz* plane. The measured HPBW was 3.4°.

polarizations were measured in the two orthogonal planes. A far-field setup was used to measure the radiation patterns and gain measurements were taken for two cardinal planes of *xz* and *yz*. The definition of each plane is illustrated in Fig. 10. After measuring both polarizations, the results were combined in post-processing to construct the LHCP and RHCP waveforms. Also, analyzed were the axial ratio and gain-bandwidth.

A comparison of the gain plots of the simulated and measured patterns yielded a close agreement of results. The *xz* plane pattern of Fig. 18 has approximately the same beamwidth of 3.3°. The *yz* plane measurement results, shown in Fig. 19, illustrate an HPBW of approximately 3.4°. The SLLs match well between measurement and simulation. However, we note that the fabrication defects discussed earlier (shown in Fig. 15) are expected to cause minor phase errors that potentially affect these levels. Note also that the LHCP and RHCP measured gains match closely to themselves and their simulated patterns.

We also compared the patterns in Figs. 18 and 19 to observe any difference in the absolute gain. The patterns show the

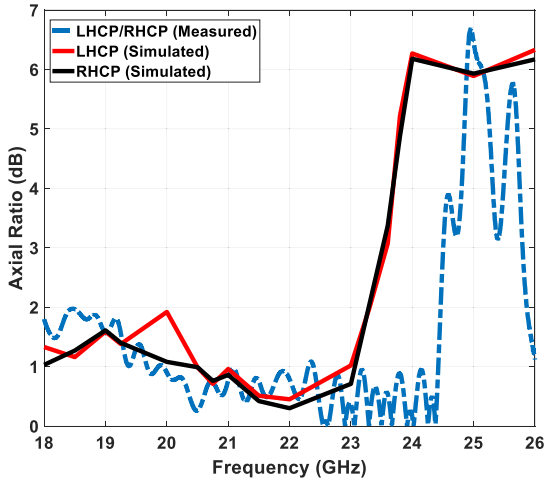

Fig. 20. Measured axial ratio of the reflectarray. The array has a bandwidth of 6.5 GHz (18–24.5 GHz) or 32.5%.

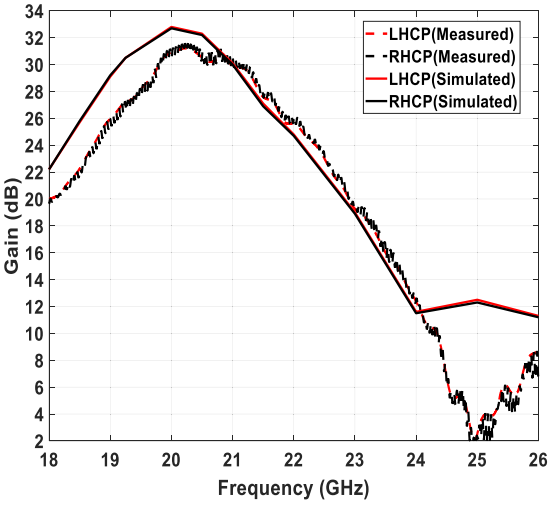

Fig. 21. Measured gain versus frequency of the reflectarray for both RHCP and LHCP and comparison with simulation results.

difference in gain that results from the 0.5 dB insertion loss of the orthomode transducer and phase errors of the reflectarray's unit cells. The simulated and measured peak gains were 32.5 and 30.8 dB, respectively. Although this corresponds to a 1.7 dB difference between the two, the difference in gains is 1.2 dB when considering the 0.5 dB insertion loss for the transducer. The inclusion of an insertion loss in the post-processing results in a real measured gain of 31.4 dB.

The measured axial ratio of the reflectarray's beam peak is shown in Fig. 20. The simulated axial ratio was 5.5 GHz or 27.5% bandwidth as compared to the 6.5 GHz or 32.5% bandwidth for the measured results. The orthomode transducer ensures that both linear polarizations stay orthogonal over the K-band with little cross-polarization and suppresses the propagation of higher-order modes. The circular aperture of the horn antenna must be correctly fed to ensure a fundamental mode propagates. As the rectangular waveguide used in our simulation did not maintain the fundamental mode over the entire K-band, the measured results of axial-ratio are better than the simulation. This resulted in a series of differences

TABLE III
COMPARISON OF METAL-ONLY DESIGNS

	This work	[5]	[4]
Element Type	Slot	Slot	Stub
Center Frequency	20 GHz	12.5 GHz	12.5 GHz
Phase Coverage	360°	360°	257°
Unit Cell Loss (Design Frequency)	0.7 dB	0.1 dB	0.4 dB
Polarization	LHCP and RHCP	Linear	Linear
Gain	31.4 dB	33.9 dB	32.5 dB
Aperture Form Factor	Circular	Circular	Circular
Aperture Size	$20\lambda_o$	$21.5\lambda_o$	$21.5\lambda_o$
Total Efficiency	35%	53.8%	–
1-dB Gain-Bandwidth	6.85%	12.8%	8.3%
3-dB Gain-Bandwidth	10.15%	–	–
Axial Ratio Bandwidth	32.5% (measured)	NA	NA

observed between the simulated and measured axial ratio at higher frequencies. Furthermore, the use of the orthomode transducer makes it possible to maintain the fundamental mode toward the higher frequencies. Regardless, the novel unit cell is able to maintain an axial ratio below 3 dB over a bandwidth far greater than its useable 1 or 3 gain bandwidth shown in Fig. 21.

VII. DISCUSSION

There are a few fabricated and measured metal-only reflectarrays to which we can compare our work. Table III lists the most notable designs. One major difference here is the lack of circular polarization support in the literature. While it is noted that both reflectarrays of [4] and [5] have higher gain than the reflectarray of this article, the difference is due to their larger array size and lower conductor losses from a much lower frequency of operation. The result is a naturally higher gain if the total efficiencies are the same, which is particularly the case in [4] as the gain is marginally higher than this article. Our work is also characterized by a 360° of phase coverage as compared to only 230° in [4]. Another noticeable difference is the higher efficiency of 53.8% in [5] while we report an efficiency of 35%. The efficiency of [5] is one of the highest reported for any metal-only reflectarray, which is primarily due to the chosen center frequency of 12.5 GHz as compared to 20 GHz for this article. The unit cell loss was 0.1 dB at 12.5 GHz versus 0.7 dB for our work at 20 GHz. At the much higher frequencies of this article, the skin depth of the incident wave is much lower which reduces the reflectarray's efficiency. This will only worsen at higher frequencies but it can be seen as a tradeoff for the mechanical and chemical properties of stainless steel. Another cause of the discrepancy may be that [5] used a different stainless-steel alloy with a different electrical conductivity than that used in this article.

The reported linearly polarized reflectarrays of Table III have 1 dB gain-bandwidths of 12.8% and 8.3%, respectively, unlike our results that are 6.85%. Of particular note in these two studies is the operation on only one polarization whereas our reflectarray operates on two. The result is an equivalent 1 dB bandwidth of 13.7% for our reflectarray. As mentioned in Section I, unlike conventional linear-polarized counterparts, this proposed reflectarray does not need a control system to manage misalignment, has a higher bandwidth, and a better reliability due to circular polarization.

VIII. Conclusion

The subject of this article was the design, fabrication, and measurement of a novel circularly polarized multi-slot metal-only reflectarray. The unit cell has a full 360° phase coverage with only a maximum loss of 0.7 dB at its center frequency of 20 GHz. The circular shape of the fabricated antenna, which was $20\lambda_o$ in diameter, made it possible to predict the behavior of this large array (1265 element) using full-wave simulation. The measured gain of this array was 31.4 dB with an aperture efficiency of 35% for both LHCP and RHCP. The 1 and 3 dB gain-bandwidth were 6.85% and 10.15%, respectively. Furthermore, the use of both of these supported circular polarization can double these values. Our measurements also closely match with the simulation results. While a metal-only reflectarray design is a good candidate for satellite applications as the use of corrosive resistant stainless steel ensures inexpensive fabrication that performs to specifications in a space environment. Our design only would be suitable for frequencies lower than the K-band due to the increased conductor losses that lower the antenna's efficiency at higher frequencies.

References

[1] D. M. Pozar, S. D. Targonski, and H. D. Syrigos, "Design of millimeter wave microstrip reflectarrays," *IEEE Trans. Antennas Propag.*, vol. 45, no. 2, pp. 287–296, Feb. 1997.

[2] R. E. Hodges, M. J. Radway, A. Toorian, D. J. Hoppe, and B. Shah, "ISARA-integrated solar array and reflectarray CubeSat deployable Ka-band antenna," presented at the Antennas Propag. Soc., Vancouver, BC, Canada, 2015.

[3] R. Wilke, K. Schraml, and D. Heberling, "Space radiation hardness of PTFE based RF substrates for GEO satellite application," presented at the 9th Eur. Conf. Antennas Propag., Lisbon Portugal, 2015.

[4] W. An, S. Xu, and F. Yang, "A metal-only reflectarray antenna using slot-type elements," *IEEE Antennas Wireless Propag. Lett.*, vol. 13, pp. 1553–1556, 2014.

[5] R. Deng, F. Yang, S. Xu, and M. Li, "A low-cost metal-only reflectarray using modified slot-type Phoenix element with 360° phase coverage," *IEEE Trans. Antennas Propag.*, vol. 64, no. 4, pp. 1556–1560, Apr. 2016.

[6] R. Deng, F. Yang, S. Xu, and M. Li, "A 100-GHz metal-only reflectarray for high-gain antenna applications," *IEEE Antennas Wireless Propag. Lett.*, vol. 15, pp. 178–181, 2016.

[7] Y. H. Cho, W. J. Byun, and M. S. Song, "High gain metal-only reflectarray antenna composed of multiple rectangular grooves," *IEEE Trans. Antennas Propag.*, vol. 59, no. 12, pp. 4559–4568, Dec. 2011.

[8] G. Carluccio, A. Mazzinghi, and A. Freni, "Design and manufacture of cosecant-squared complementary reflectarrays for low-cost applications," *IEEE Trans. Antennas Propag.*, vol. 65, no. 10, pp. 5220–5227, Oct. 2017.

[9] R. Deng, S. Xu, F. Yang, and M. Li, "Design of a low-cost single-layer X/Ku dual-band metal-only reflectarray antenna," *IEEE Antennas Wireless Propag. Lett.*, vol. 16, pp. 2106–2109, 2017.

[10] H. Al-Saedi, W. M. Abdel-Wahab, S. Gigoyan, S. Safavi-Naeini, and R. Mittra, "A metal-only reflectarray antenna element with wide angular response based on spiral slots," in *Proc. IEEE Int. Symp. Antennas Propag. USNC/URSI Nat. Radio Sci. Meeting*, Jul. 2018, pp. 1635–1636.

[11] K. Q. Henderson and N. Ghalichechian, "Metal only spiral slot reflectarray element operating at 66 GHz," in *Proc. IEEE Int. Symp. Antennas Propag. USNC/URSI Nat. Radio Sci. Meeting*, Jul. 2018, pp. 1633–1634.

[12] A. Yu, F. Yang, A. Z. Elsherbeni, J. Huang, and Y. Rahmat-Samii, "Aperture efficiency analysis of reflectarray antennas," *Microw. Opt. Technol. Lett.*, vol. 52, no. 2, pp. 364–372, Feb. 2010.

[13] M. Żebrowski, "Illumnatation and Spillover efficiency calculations for rectangular reflectarray antennas," *High Freq. Electron.*, vol. 11, no. 12, pp. 28–38, Dec. 2013.

[14] J. Huang and J. A. Encinar, *Reflectarray Antennas*. Hoboken, NJ, USA: Wiley, 2008.

[15] H. Rajagopalan, S. Xu, and Y. Rahmat-Samii, "On understanding the radiation mechanism of reflectarray antennas: An insightful and illustrative approach," *IEEE Antennas Propag. Mag.*, vol. 54, no. 5, pp. 14–38, Oct. 2012.

[16] J. A. Zornoza and J. A. Encinar, "Efficient phase-only synthesis of contoured-beam patterns for very large reflectarrays," *Int. J. RF Microw. Comput.-Aided Eng.*, vol. 14, no. 5, pp. 415–423, Sep. 2004.

[17] Y. Mao, S. Xu, F. Yang, and A. Z. Elsherbeni, "A novel phase synthesis approach for wideband reflectarray design," *IEEE Trans. Antennas Propag.*, vol. 63, no. 9, pp. 4189–4193, Sep. 2015.

[18] G. Ahmad, T. W. C. Brown, C. I. Underwood, and T. H. Loh, "An efficient algorithm for electrically large reflectarray antenna design automation," presented at the Int. Workshop Electromagn., Appl. Student Innov. Competition, London, U.K., 2017.

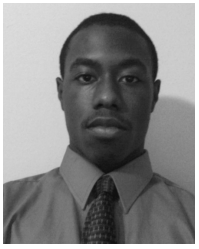

Kendrick Q. Henderson (Student Member, IEEE) received the B.S. degree in electrical engineering, the B.S. degree in computer engineering, and the M.S. degree in electrical engineering from the University of South Alabama, Mobile, AL, USA, in 2015, 2015, and 2017, respectively. He is currently pursuing the Ph.D. degree with the ElectroScience Laboratory, Department of Electrical and Computer Engineering, The Ohio State University, Columbus, OH, USA.

He is an employee of the Radar Division, Naval Surface Warfare Center-Crane, Crane, IN, USA. He has authored several conference and journal articles throughout his time as an undergraduate and graduate student. His research interests include reflectarrays, metasurfaces, phased arrays, waveguide-based antennas, and beamforming techniques for radar applications.

Mr. Henderson was a recipient of the 2017 Department of Defense SMART Scholarship.

Nima Ghalichechian (Senior Member, IEEE) received the Ph.D. degree in electrical engineering from the University of Maryland, College Park, MD, USA.

He developed MEMS electrostatic micromotors supported on microball bearings at the University of Maryland. From 2007 to 2012, he was with the Research Department of FormFactor, Inc., Livermore, CA, USA, as a Senior Principal Engineer. During this period, he helped to design and develop MEMS microsprings for advanced probe cards used in testing memory and SoC semiconductor devices. He joined The Ohio State University, Columbus, OH, USA, as a Research Scientist, in 2012. As a Principal Investigator, he established several new programs sponsored by NSF, DARPA, and AFRL. From 2016 to 2017, he held a Research Assistant Professor position. He transitioned into an Assistant Professor position in August 2017. He is currently an Assistant Professor at the Department of Electrical and Computer Engineering and the ElectroScience Laboratory, The Ohio State University. He is currently a Principal Investigator and the Director of the RF Microsystems Laboratory and advises seven doctoral and two masters' students. His research interests include phase-change materials, reconfigurable antennas, arrays, UWB antennas, millimeter-wave systems, meta-surfaces, 3-D-printed antennas, novel materials, and microfabrication techniques.

Dr. Ghalichechian was a recipient of the 2019 NSF CAREER Award, the 2019 Air Force Research Laboratory Summer Faculty Fellowship Award, and the 2018 Ohio State University Lumley Research Award.